Multiple deformation mechanisms of Ti–22.4Nb–0.73Ta–2.0Zr–1.34O alloy

Y. Yang,[1,2,a)] G. P. Li,[1,b)] G. M. Cheng,[1,2] Y. L. Li,[1] and K. Yang[1]
[1]*Institute of Metal Research, Chinese Academy of Sciences, 72 Wenhua Road, Shenyang 110016, People's Republic of China*
[2]*Graduate School, Chinese Academy of Sciences, Beijing 100039, People's Republic of China*

(Received 11 December 2008; accepted 15 January 2009; published online 9 February 2009)

Ti–22.4Nb–0.73Ta–2.0Zr–1.34O (at. %) alloy after cold compression to ~5.2% strain was investigated. The alloy exhibited multiple plastic deformation mechanisms, including the stress-induced α'' martensitic (SIM α'') and ω phase transformations, $1/2\langle 111\rangle$ dislocations slipping on the $\{112\}\beta$ planes as well as $\{332\}\langle 113\rangle\beta$ and $\{112\}\langle 111\rangle\beta$ twinning, which have not previously been reported to coexist in a titanium alloy. It was also found that β phase with the {200} planes vertical to the compression direction was almost completely consumed away by a $\beta \rightarrow$ SIM α'' transformation, and a (100) texture of SIM α'' formed. © *2009 American Institute of Physics*. [DOI: 10.1063/1.3078521]

The deformation behaviors of metastable β and β titanium alloys have been reported to be closely related to the stability of the parent phase. Controlling the phase stability, stress-induced α'' martensitic (SIM α'') and ω phase transformations, $\{332\}\langle 113\rangle\beta$ and $\{112\}\langle 111\rangle\beta$ deformation twinning and slip are operative.[1–8] In past several years, gum metals, a group of the least stable β titanium alloys, have been developed for their advantages of multifunctional properties after severe cold deformation.[9] Saito *et al.*[9] suggested that the unique properties are produced by a dislocation-free plastic deformation mechanism called giant planar faults, which induce crystallographic rotations 10°–30° from the neighboring area by plastic deformation.[9–13] The calculations of Li *et al.*[14] supported the concept that the triggering stress for dislocation motion exceeded the ideal strength of gum metal. This could result in the plastic deformation through the giant planar faults accompanied by nanodisturbances, a kind of nanoscale dipoles of nonconventional partial dislocations with arbitrary and nonquantized Burgers vectors.[15] However, recent work has shown that more conventional deformation mechanisms are still operative in the gum metals,[16–21] for example, largely reversible stress-induced phase transformation during tensile loading and unloading was observed using *in situ* synchrotron x-ray diffraction (SXRD),[20,21] and $1/2\langle 111\rangle$ dislocations were observed in the severely cold-swaged Ti–23Nb–0.7Ta–2Zr–1.2O (at. %) alloy[16] and in annealed cold-swaged gum metal.[17] In our previous work,[18] both the SIM α'' and $\{112\}\langle 111\rangle\beta$ deformation twins were found in a cold-compressed Ti–22.4Nb–0.73Ta–2.0Zr–1.34O (at. %) alloy with 77% reduction in height, which exhibited properties similar to those of gum metals. Such twinning mechanism also occurred in gum metal.[19,21] Additionally, the stress-induced ω phase was found in Ti–23Nb–0.7Ta–2Zr–1.2O alloy.[19,21] The above results suggested that the multiple deformation mechanisms, except for $\{332\}\langle 113\rangle\beta$ twinning, occurred in the gum metal. In this letter, Ti–22.4Nb–0.73Ta–2.0Zr–1.34O (at. %) alloy with a small strain of ~5.2% reduction in height was investigated using optical microscope (OM), XRD, transmission electron microscope (TEM), and electron-backscatter diffraction (EBSD). The alloy exhibited multiple plastic deformation mechanisms, including the stress-induced α'' martensitic and ω phase transformations, $1/2\langle 111\rangle$ dislocations slipping on the $\{112\}\beta$ planes as well as $\{332\}\langle 113\rangle\beta$ and $\{112\}\times\langle 111\rangle\beta$ twinning, which have not been reported previously to coexist in a titanium alloy.

The alloy was melted three times using a nonconsumable arc-melting furnace under argon protection. The ingot with composition of Ti–22.4Nb–0.73Ta–2.0Zr–1.34O (at. %) was forged at 1080 and 750 °C, and then homogenized at 950 °C for 30 min followed by ice water quenching. Uniaxial compression was conducted at room temperature with a constant crosshead speed of 0.01 mm/s (initial strain rate of 1.18×10^{-3} s^{-1}). Optical microstructure observations were performed on an Axiovert200 MAT OM. An S-3400N scanning electron microscope (SEM), equipped with HKL CHANNEL 5 software, was employed to observe the morphologies and conduct EBSD analysis. The samples for OM, SEM, and EBSD were electropolished and then etched. Phase constitutions were detected by a Rigaku D/max-2400PC x-ray diffractometer using Cu $K\alpha$ working at voltage of 56 kV and current of 182 mA. TEM analysis was performed on a Tecnai G^2 20 TEM operating at 200 kV. TEM foils were mechanically thinned to ~30 μm in thickness and further reduction was carried out using a Tenupol-5 twin-jet electrolytic polisher in a solution of 6% perchloric acid+35% butyl alcohol+59% methanol (vol %) at −10 to −20 °C and 10 V.

Optical microstructure observations showed that the solution-treated alloy exhibits a typical equiaxed microstructure with single β phase [Figs. 1(a) and 1(c)] and that the cold compression induces groups of parallel thin lines and a few of thick laths in the original β grains [Fig. 1(b)]. A small amount of SIM α'' was detected by XRD analysis after compression [Figs. 1(d) and 1(e)]. The SIM α'' exhibits a (100) texture, as evidenced by the $(200)\alpha''$ peak [Fig. 1(d)] and weak $(021)\alpha''$ peak [Fig. 1(e)] in the XRD profiles taken from the planes vertical and parallel to the compression direction, respectively. Meanwhile, $I_{\{200\}\beta}/I_{\{110\}\beta}$, the ratio of intensities of $\{200\}\beta$ and $\{110\}\beta$ peaks, dropped from about

a)Electronic mail: yiyang@imr.ac.cn.
b)Author to whom correspondence should be addressed. Tel.: +86 24 83978619. FAX: +86 24 23902021. Electronic mail: gpli@imr.ac.cn.

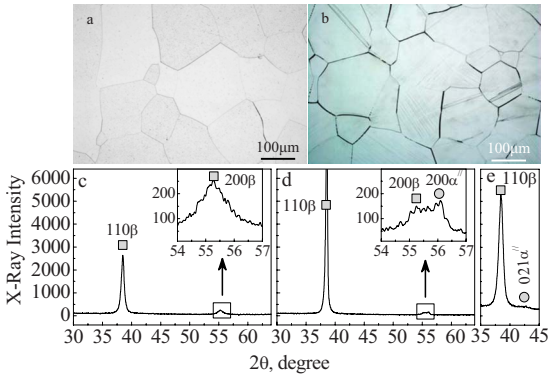

FIG. 1. (Color online) Optical microstructures and XRD profiles of solution-treated [(a) and (c)] and cold-compressed specimens [(b), (d), and (e)]. Insets in (c) and (d) are enlargements of the rectangular zones. Scanned planes of the deformed sample were vertical (d) and parallel (e) to the compression direction, respectively.

0.1 to 0.016 before [Fig. 1(c)] and after [Fig. 1(d)] compression. This indicated that the β phase with {200} plane vertical to the compression direction was almost completely consumed away by $\beta \rightarrow$ SIM α'' transformation during the compression. The above results could be interpreted by the orientation relationship between β and α'' phases, i.e., $(110)\beta//(001)\alpha''$ and $[001]\beta//[100]\alpha''$.[22–25] As the $\beta \rightarrow \alpha''$ transformation occurs, the $[001]\beta$ direction shrinks to form $[100]\alpha''$ and the $[\bar{1}10]\beta$ direction expands to form $[010]\alpha''$.[22–25] Therefore, the SIM α'' transformation prefers to take place in the β phase with {200} plane vertical to the compression direction.

Besides the SIM α'', sheetlike stress-induced ω phase was also found (Fig. 2). The orientation relationship between the ω phase and β parent matrix is $[311]\beta//[11\bar{2}3]\omega$ and $(01\bar{1})\beta//(0\bar{1}11)\omega$. However, the stress-induced ω phase was too low in volume fraction to be detected by XRD [Figs. 1(d) and 1(e)].

Many dislocations were also observed in the compressed alloy (Fig. 3). Assuming that the electron beam was vertical to dislocation lines, the dislocations in Fig. 3(b) were parallel to $[11\bar{1}]\beta$ direction on $(112)\beta$ plane and $[111]\beta$ direction on $[11\bar{2}]\beta$ plane, respectively; those in Fig. 3(d) were parallel to $[\bar{1}10]\beta$ direction on $(11\bar{2})\beta$ plane, $[01\bar{1}]\beta$ direction on $(2\bar{1}\bar{1})\beta$ plane and $[10\bar{1}]\beta$ direction on $(\bar{1}2\bar{1})\beta$ plane, respectively. They were identified as belonging to $\langle 111\rangle\{112\}$ slip

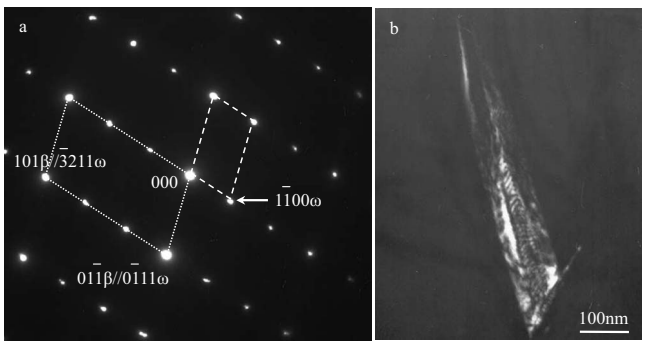

FIG. 2. Stress induced ω phase in the cold-compressed alloy. (a) Selected area diffraction (SAD) pattern of $[311]\beta//[11\bar{2}3]\omega$ zone axis. (b) Dark field image using the arrowed diffraction spot $((1\bar{1}00)\omega)$ in (a).

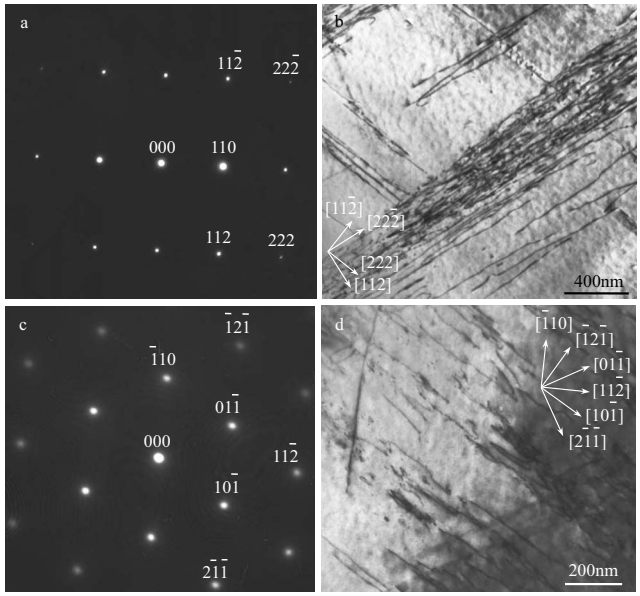

FIG. 3. $1/2\langle 111\rangle$ dislocations on the $\{112\}\beta$ planes. (a) and (c) are the SAD patterns of $[1\bar{1}0]\beta$ and $[111]\beta$ zone axes; (b) and (d) are the corresponding bright-field TEM images.

systems. $\langle 111\rangle\{110\}$ and $\langle 111\rangle\{123\}$ glides were not observed. This is because $\langle 111\rangle\{112\}$ slipping is the easiest system in bcc metal at room temperature.

EBSD was used to characterize the thick laths shown in Fig. 1(b). Crystallographic misorientations between almost all the visible thick laths and the matrix (CMLM) were detected. Although the directions and sizes of thick laths were irregular, the CMLMs were uniform, and all the CMLM were about 50.5° [Figs. 4(a) and 4(b)]. Since the crystallographic misorientations of the matrix with $\{332\}\langle 113\rangle\beta$ twins and $\{112\}\langle 111\rangle\beta$ twins are 50.5° and 70.3° around $\langle 110\rangle\beta$,

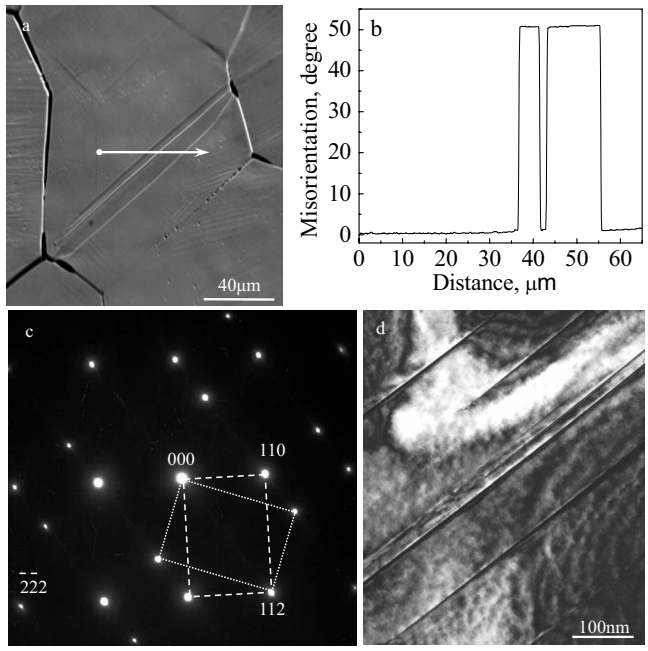

FIG. 4. Twins in the slightly cold-compressed alloy. (a) SEM image of $\{332\}\langle 113\rangle\beta$ twins; (b) Misorientations relative to the first points along the arrow in (a); (c) The SAD pattern of $[1\bar{1}0]\beta$ zone axis; (d) Morphology of $\{112\}\langle 111\rangle\beta$ twins corresponding to (c).

respectively,[1,18] the thick laths in the compressed alloy were $\{332\}\langle 113\rangle\beta$ twins. Furthermore, some slab-sided $\{112\}\times\langle 111\rangle\beta$ twins with the thickness of about 10 nm were found under TEM [Figs. 4(c) and 4(d)], the same as those observed previously in the severely cold-compressed alloy.[18]

Generally, the deformation behaviors of metastable β and β titanium alloys are closely related to the stability of β phase. The plastic deformation mode changes from the stress-induced martensite to twin to slip mechanism as the stability of the β phase increases.[22,26,27] For Ti–Nb–Ta–Zr–O system, Kuramoto *et al.*[11] observed $\{332\}\langle 113\rangle\beta$ deformation twinning and Furuta *et al.*[12] found SIM α'' in Ti–21Nb–0.7Ta–2Zr–1.2O (at. %) alloy with lower bcc stability. In Ti–23Nb–0.7Ta–2Zr–1.2O (at. %) alloy (gum metal), Talling *et al.*[20,21] and Xing *et al.*[16] and Xing and Sun[19] reported SIM α'' transformation, $1/2\langle 111\rangle$ dislocations slipping, stress-induced ω phase transformation as well as $\{112\}\langle 111\rangle\beta$ twinning. Kuramoto *et al.*[11] only found dislocation glide in Ti–25Nb–0.7Ta–2Zr–1.2O (at. %) alloy. The above results show that the deformation mechanism of Ti–Nb–Ta–Zr–O system is dependent on the composition. However, the boundaries between different mechanisms are not quite clear. Especially, Ti–22.4Nb–0.73Ta–2Zr–1.34O (at. %) alloy exhibits all deformation mechanisms mentioned above, which have not been reported previously to coexist in a titanium alloy. This indicates the critical composition for $\{332\}\langle 113\rangle\beta$ twinning in Ti–Nb–Ta–Zr–O system.

In summary, Ti–22.4Nb–0.73Ta–2.0Zr–1.34O (at. %) alloy exhibits multiple plastic deformation mechanisms after cold compression of ~5.2% reduction in height. The stress-induced α'' martensitic and ω phase transformations, $1/2\langle 111\rangle$ dislocations slipping on the $\{112\}\beta$ planes and $\{332\}\langle 113\rangle\beta$ and $\{112\}\langle 111\rangle\beta$ twinning coexist, and this has not been reported previously in a titanium alloy. Moreover, $\beta\rightarrow$SIM α'' transformation takes place preferentially in the β phase with {200} plane vertical to the compression direction, which results in the near complete removal of β phase having this orientation and formation of SIM α'' with a (100) texture in this stage.

[1] N. Sakaguch, M. Niinomi, and T. Akahori, Mater. Trans. **45**, 1113 (2004).
[2] T. Grosdidier and M. J. Philippe, Mater. Sci. Eng., A **291**, 218 (2000).
[3] W. Xu, K. B. Kim, J. Das, M. Calin, and J. Eckert, Scr. Mater. **54**, 1943 (2006).
[4] S. Hanada and O. Izumi, Metall. Trans. A **11**, 1447 (1980).
[5] S. Hanada and O. Izumi, Metall. Trans. A **18**, 265 (1987).
[6] S. Hanada, M. Ozeki, and O. Izumi, Metall. Trans. A **16**, 789 (1985).
[7] D. Kuroda, M. Niinomi, M. Morinaga, Y. Kato, and T. Yashiro, Mater. Sci. Eng., A **243**, 244 (1998).
[8] L. Q. Wang, W. J. Lu, J. N. Qin, F. Zhang, and D. Zhang, Mater. Sci. Eng., A **490**, 421 (2008).
[9] T. Saito, T. Furuta, J. H. Hwang, S. Kuramoto, K. Nishino, N. Suzuki, R. Chen, A. Yamada, K. Ito, Y. Seno, T. Nonaka, H. Ikehata, N. Nagasako, C. Iwamoto, Y. Ikuhara, and T. Sakuma, Science **300**, 464 (2003).
[10] J. Hwang, S. Kuramoto, T. Furuta, K. Nishino, and T. Saito, J. Mater. Eng. Perform. **14**, 747 (2005).
[11] S. Kuramoto, T. Furuta, J. H. Hwang, K. Nishino, and T. Saito, J. Jpn. Inst. Met. **69**, 953 (2005).
[12] T. Furuta, S. Kuramoto, J. H. Hwang, K. Nishino, and T. Saito, Mater. Trans. **46**, 3001 (2005).
[13] S. Kuramoto, T. Furuta, J. H. Hwang, K. Nishino, and T. Saito, Metall. Mater. Trans., A **37**, 657 (2006).
[14] T. S. Li, J. W. Morris, Jr., N. Nagasako, S. Kuramoto, and D. C. Chrzan, Phys. Rev. Lett. **98**, 105503 (2007).
[15] M. Y. Gutkin, T. Ishizaki, S. Kuramoto, and I. A. Ovid'ko, Acta Mater. **54**, 2489 (2006).
[16] H. Xing, J. Sun, Q. Yao, W. Y. Guo, and R. Chen, Appl. Phys. Lett. **92**, 151905 (2008).
[17] W. Y. Guo, H. Xing, J. Sun, X. L. Li, J. S. Wu, and R. Chen, Metall. Mater. Trans., A **39**, 672 (2008).
[18] Y. Yang, G. P. Li, G. M. Cheng, H. Wang, M. Zhang, F. Xu, and K. Yang, Scr. Mater. **58**, 9 (2008).
[19] H. Xing and J. Sun, Appl. Phys. Lett. **93**, 031908 (2008).
[20] R. J. Talling, R. J. Dashwood, M. Jackson, S. Kuramotoc, and D. Dye, Scr. Mater. **59**, 669 (2008).
[21] R. J. Talling, R. J. Dashwood, M. Jackson, and D. Dye, "On the mechanism of superelasticity in gum metal," Acta Mater. (in press).
[22] H. Y. Kim, Y. Ikehara, J. I. Kim, H. Hosoda, and S. Miyazaki, Acta Mater. **54**, 2419 (2006).
[23] T. W. Duerig, J. Albrecht, D. Richter, and P. Fischer, Acta Metall. **30**, 2161 (1982).
[24] M. Grujicic and C. P. Narayan, Mater. Sci. Eng., A **151**, 217 (1992).
[25] T. Furuta, S. Kuramoto, R. Chen, J. H. Hwang, K. Nishino, T. Saito, and M. Ikeda, J. Jpn. Inst. Met. **70**, 579 (2006).
[26] H. S. Kim, S. H. Lim, I. D. Yeo, and W. Y. Kim, Mater. Sci. Eng., A **449**, 322 (2007).
[27] M. Abdel-Hady, K. Hinoshita, and M. Morinaga, Scr. Mater. **55**, 477 (2006).